URSI GASS 2021, Rome, Italy, 28 August - 4 September 2021

A Generalized Anisotropic Power-Law Roughness Spectrum and Its Applications to Radar Backscattering from Soil Surfaces

Ying Yang(1), Kun-Shan Chen* (1) (2)
(1) Guilin University of Technology, Guangxi, 532100, China
(2) Aerospace Information Research Institute, Chinese Academy of Sciences, Beijing 100101, China

Abstract

We present a generalized power-law roughness spectrum to account for the spatial anisotropy. For completeness, both the correlation anisotropy and the scaling anisotropy are included. The spatial anisotropy is essential to correctly interpret the radar scattering from an agriculture field where both plow and sow practice. The dependence of the backscattering coefficient on the correlation anisotropy and the scaling anisotropy is investigated through a model simulation. Drastic change of backscattering strength is observed due to the anisotropy. The correlation anisotropy and the scaling anisotropy generate similar backscattering angular behavior, implying that in the context of spatial anisotropy, merely using correlation length in scattering modeling is insufficient. Equivalently, the correlation length retrieved from the backscattering coefficients perhaps is not unique. A fair use of the generalized anisotropic power-law roughness spectrum in conjunction with the scattering model is illustrated by comparing the backscattering coefficients with experimental measurements.

1 Introduction

Microwave remote sensing of soil moisture on either a regional or global scale has been of great interest to contribute to weather forecast, climate changes, and energy cycle studies[1]. Efforts have been devoted to better understanding the wave-soil surface interactions and, consequently, a more accurate retrieval of soil moisture from microwave observations [2-4]. In these regards, in forward modeling, namely, the electromagnetic scattering model, be it theoretical or empirical, or hybrid, of rough soil surface, is vital. A fair use of the scattering model requires an appropriate description of the soil surface being observed [5-7]. Either fractal or classic l-s approach has been successfully applied [8]. Inappropriate modeling of surface roughness, including the rms height, correlation length, and roughness spectrum, usually leads to large deviation between model prediction and in-situ measurements [9].

Previous studies show that the soil surfaces are better represented by the fractal surface or power law spectrum [10-11]. A generalized power-law roughness spectrum was proposed and used in IEM model simulations, showing a good agreement of backscattering coefficient with most experimental measurements [12]. To account for the spatial anisotropy, this study extends the power-law roughness spectrum in two aspects: directional correlation lengths and directional scaling factors. We first show the characteristics of the generalized two-dimensional anisotropic roughness spectrum in terms of correlation anisotropy and scaling anisotropy, defined by the ration of correlation lengths and scaling factors, respectively. The correlation lengths and the scaling factors, either together or separately, determine the spatial anisotropy. The dependence of radar scattering on either correlation length anisotropy or scaling anisotropy is then examined. In the end, we apply the proposed anisotropic power-law roughness spectrum in conjunction with the AIEM scattering model [8] to interpret the measurements.

2 A Generalized Anisotropic Power-Law Roughness Spectrum

For a stationary, ergodic randomly rough surface, a power-law spectrum (or power spectral density, PSD), as given in [12], maybe generalized to be of the form:

$$S(K_x,K_y)=\frac{2\sigma^2\ell_x\ell_y\Gamma(\alpha_x+1/2)\Gamma(\alpha_y+1/2)}{\Gamma(\alpha_x)\Gamma(\alpha_y)[1+(K_x\ell_x)^2]^{\alpha_x+1/2}[1+(K_y\ell_y)^2]^{\alpha_y+1/2}} \quad (1)$$

where σ is the RMS height, ℓ_x,ℓ_y the correlation lengths along x and y directions, respectively; α_x,α_y are scaling factors controlling the power-law decaying rates in orthogonal x and y directions, respectively; $\Gamma(x)$ is the Gamma function.

The correlation lengths and the scaling factors, either together or separately, determine the spatial anisotropy. Fig. 1 displays the isotropic surface (a) and anisotropic surface (b). A generalized power law spectrum with different correlation lengths ℓ_x,ℓ_y and scaling factors α_x,α_y are given in Fig. 2.

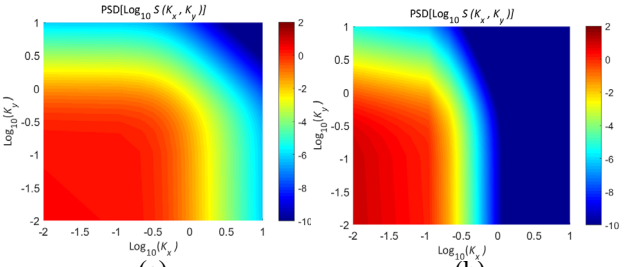

(a) (b)

Figure 1. A generalized power law spectrum with (a): ℓ_x=ℓ_y=2; $\alpha_x = \alpha_y = 2$; (b): ℓ_x=2,ℓ_y=6; $\alpha_x = 2, \alpha_y = 6$.

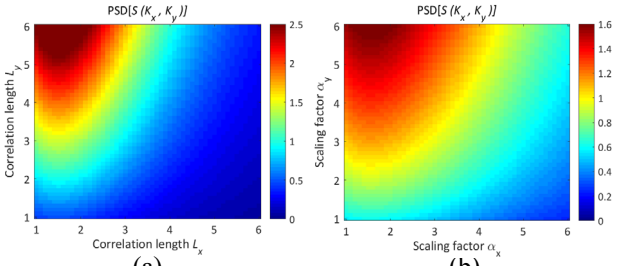

(a) (b)

Figure 2. A generalized power law spectrum with different correlation lengths ℓ_x, ℓ_y along x and y directions and scaling factors α_x, α_y. (a): α_x=2, α_y=2, (a): ℓ_x=2, ℓ_y=2.

By Wiener–Khinchin theorem, the covariance function and the power spectral density (PSD) are related by the Fourier transform. For a randomly rough surface, the PSD represents the roughness spectrum. For second-order statistics, it is the variance distribution over the whole wavenumber domain $\mathbf{K} = (K_x, K_y)$:

$$C(r_x, r_y) = \frac{1}{2\pi}\int_{-\infty}^{\infty} S(K_x, K_y) e^{j(K_x r_x + K_y r_y)}\, dK_x K_y \quad (2a)$$

$$S(K_x, K_y) = \frac{1}{2\pi}\int_{-\infty}^{\infty} C(r_x, r_y) e^{-j(K_x r_x + K_y r_y)}\, dr_x r_y \quad (2b)$$

where r_x, r_y are lag distances along x and y directions, respectively. Substituting (1) into (2a), we have the covariance function:

$$C(r_x, r_y) = \frac{4\sigma^2}{\Gamma(\alpha_x)\Gamma(\alpha_y)} [\frac{r_x}{2\ell_x}]^{\alpha_x} [\frac{r_y}{2\ell_y}]^{\alpha_y} K_{\alpha_x}(\frac{r_x}{\ell_x}) K_{\alpha_y}(\frac{r_y}{\ell_y}) \quad (3)$$

where $K_\alpha(x)$ is α^{th}-order modified Bessel function.

The correlation function $\rho(x,y) = C(x,y)/\sigma^2$ is given by

$$\rho(x,y) = \frac{4}{\Gamma(\alpha_x)\Gamma(\alpha_y)} [\frac{x}{2\ell_x}]^{\alpha_x} [\frac{y}{2\ell_y}]^{\alpha_y} K_{\alpha_x}(\frac{x}{\ell_x}) K_{\alpha_y}(\frac{y}{\ell_y}) \quad (4)$$

When $\ell_x = \ell_y = \ell$, $\alpha_x = \alpha_y = \alpha$, the correlation function reduces into isotropic:

$$\rho(r) = \frac{2}{\Gamma(\alpha)} [\frac{r}{2\ell}]^{\alpha} K_\alpha(\frac{r}{\ell}) \quad (5)$$

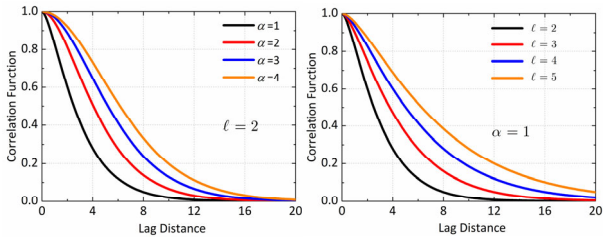

Figure 3. Correlation function with different correlation lengths ℓ and scaling factors α: (a): ℓ=2, α=1, 2, 3, 4, (b): α=1, ℓ=2, 3, 4, 5.

From the plots shown in Fig. 3, we see that the correlation function's decaying rates with lag distance can be controlled by either correlation lengths or the scaling factors. Together with Figs. 1-2, we expect the scattering strength is dependent on the surface roughness through the spectral form, correlation lengths, and scaling factors. Compared to the conventional use of only correlation lengths, the scaling factors add more freedom to predict the scattering. Meanwhile, they also complicate further to model the rough surface in the context of soil moisture sensing. In what follows, we present the backscattering dependences on the correlation lengths and the scaling factors.

3 Model Results of Backscattering Coefficients

For numerical illustrations, we apply the AIEM scattering model to simulate the backscattering coefficients at L-band (1.25GHz).

3.1 Influence of Scaling Factors

By varying the correlation length and the scaling factor, we plot the backscattering coefficient at incident angle from 0° to 60°, as shown in Fig.4 for both HH and VV polarizations. For a fixed correlation length ℓ_x=ℓ_y=5cm and scaling factor α_x=1, the backscattering increases with increased scaling factor in y- direction, which is readily understood from that $\sigma^\circ \propto S(2k\sin\theta_i, 0)$ (see (1)).

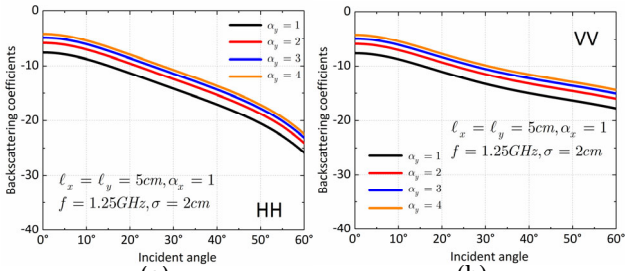

(a) (b)

Figure 4. Backscattering coefficients from isotropic (black line) and anisotropic surface as function of incident angle. ℓ_x=ℓ_y=5cm, α_x=1, ε_r=12 − j1.05, f=1.25GHz, σ=2cm, (a) HH polarization. (b) VV polarization.

When we reverse the role of α_x and α_y as those in Fig.4, we have the backscattering coefficients as plotted in Fig. 5. We see that the angular trend for both HH and VV polarizations is now much more strongly dependent on the scaling factor in x- direction. To examine the influence of scaling factors more clearly, in Fig. 6, we plot the backscattering coefficients at incident angle of 30° for α_x from 1-6 while fix α_y at 2, and vice versa. From Fig. 6 (a), we note that the increasing of α_x quickly reduces the backscattering; the drop rates for HH and VV polarizations are almost the same. The sensitivity of the backscattering coefficient to the scaling factor α_x is relatively high. The increasing backscattering with α_y is evident from Fig. 6 (b). Note that the role of scaling

factors α_x α_y in affecting the scattering depends on the radar observation geometry.

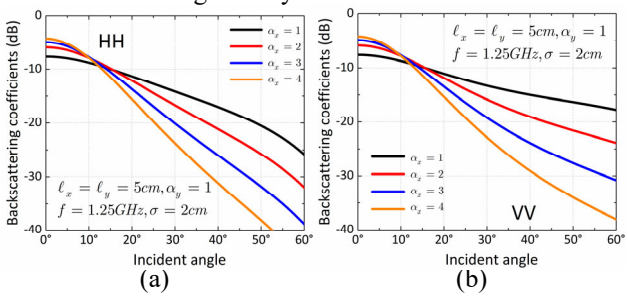

(a) (b)

Figure 5 . Backscattering coefficients from isotropic (black line) and anisotropic surface as function of incident angle. ℓ_x=ℓ_y=$5cm$, α_y=1 , ε_r=$12-j1.05$, f=$1.25GHz$, σ=$2cm$, (a) HH polarization. (b) VV polarization.

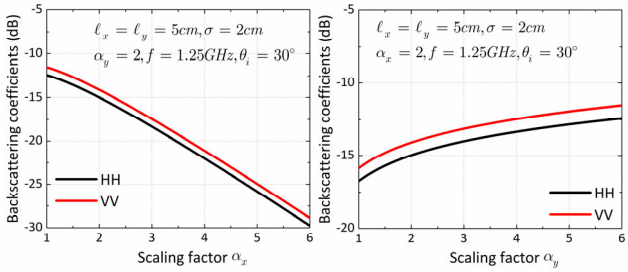

(a) (b)

Figure 6. Influence of scaling factors α_x, α_y on backscattering coefficients with ℓ_x=ℓ_y=$5cm$, ε_r=$12-j1.05$, f=$1.25GHz$, σ=$2cm$, θ_i=$30°$ (a): $\alpha_x = 1 \sim 6, \alpha_y = 2$ (b): $\alpha_x = 2, \alpha_y = 1 \sim 6$.

3.2 Influence of Correlation Lengths

Similar to the analysis of scaling factors effect, we examine the backscattering dependence on correlation lengths. To do so, we fix the scaling factors at 2. We first show the dependence of the backscattering coefficient on ℓ_x while keeping ℓ_y=$5cm$ in Fig.7 (a), and then swap the role of ℓ_x and ℓ_y to obtain the results given in Fig.7 (b). Quantitively, the larger the correlation length ℓ_x , the smaller the backscattering coefficient, as it should be for the surface slope is smaller. When the radar observation direction is orthogonal to y-direction, the presence of correlation length ℓ_x is to increase the backscattering coefficient, as illustrated in Fig. 7 (b). The effect is similar to that by the y-direction scaling factor α_y.

The above discussion suggest that the correlation anisotropy and the scaling anisotropy generate similar backscattering angular behavior, implying that in the context of spatial anisotropy, merely using correlation length in scattering modeling is insufficient. Equivalently, the correlation length retrieved from the backscattering coefficients perhaps is not unique, and thus only "effective correlation length" retrieval is possible [13].

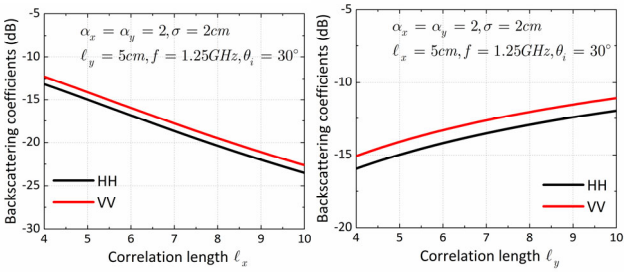

(a) (b)

Figure 7. Influence of correlation lengths ℓ_x, ℓ_y on the backscattering coefficients with α_x=α_y=2 , ε_r=$12-j1.05$, f=$1.25GHz$, σ=$2cm$, θ_i=$30°$ (a) ℓ_x=$4 \sim 10cm, \ell_y$=$5cm$ (b). ℓ_x=$5cm, \ell_y$=$4 \sim 10cm$.

4 Comparison of Backscattering Coefficients with Experimental Data

The first measurement data [14] for comparison was acquired at central frequency 5.3 GHz, and incident angle varying from 10° to 60° with a step of 10° , over plowed soil surface, which was a clay loam with 27.2% clay, 61.75% loam, 11.05% sand, and 1.7 organic matter. Over the measurement period, the soil moisture content was considered stable 0.153. From Fig.8, we note that the model predictions at both HH and VV polarizations well match the measured data. The second set of data for comparison were collected at C- and X-bands, HH and VV polarization, from 25° to 57° [15]. The experimental site had different ploughed soil practices for future cultures (corn, sugar beet, etc.), and the soil texture was 17% clay, 78% limon, and 5% sand; the soil moisture was about 0.35. As shown in Fig.9, we see that the model predictions with the anisotropic spectrum are in good agreement with the measurement data. The results demonstrate that the anisotropic pow-law spectrum is practically useful to characterize the bare agricultural soils' backscattering, especially for the plowed soil practices.

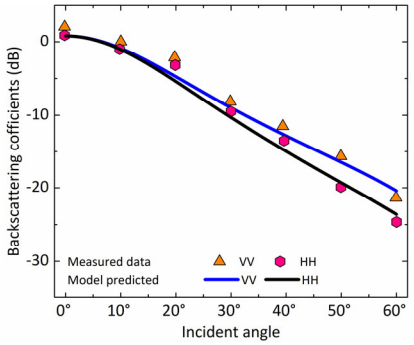

Figure 8. Comparison of the backscattering coefficients between model predictions and measurements [14]: ℓ_x=$1cm, \ell_y$ = $6cm$, α_x=$2.5, \alpha_y$=6 , m_v=0.153 , σ=$0.3cm$, f=$5.3GHz$.

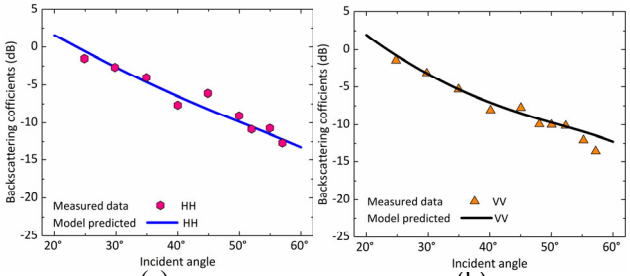

Figure 9. Comparison of the backscattering coefficients between model predictions and measurements [15]: ℓ_x=1cm, ℓ_y = 6cm , α_y=6 , m_v=0.35 , σ=0.6cm , (a): f=5.3GHz , α_x=2.5, HH polarization, (b) f=9.6GHz , α_x=1.8, VV polarization.

5 Conclusions

We investigate a generalized power-law roughness spectrum to account for spatially anisotropic effect in wave scattering from agricultural soil surfaces where roughness is disturbed due to plowing and sowing practice. The roughness spectrum model contains correlation anisotropy and scaling anisotropy, which gives a higher degree of freedom to adjust the parameters for matching the backscattering measurements, as demonstrated in two independent data sets. However, it complicates the roughness description in terms of surface parameters retrieval because similar backscattering angular behavior can be generated by combining different correlation anisotropy and scaling anisotropy. Results suggest that it should better configure a radar observation geometry to minimize the spatial anisotropy influence if the soil moisture is of primary interest. Further investigation into the bistatic scattering in the context of spatial anisotropy effects should be pursued.

6 References

1. J. Shukla and Y. Mintz, "Influence of Land-Surface Evapotranspiration on The Earth's Climate," *Science*, **215**, 4539, April, 2182, pp. 1498–1501, doi: 10.1126/science.215.4539.1498.

2. S. Paloscia, G. Macelloni, E. Santi, et al, "A Multifrequency Algorithm for the Retrieval of Soil Moisture on A Large Scale Using Microwave Data from SMMR and SSM/I Satellites," *IEEE Transactions on Geoscience and Remote Sensing*, **39**, 8, August, 2001, pp. 1655–1661, doi: 10.1109/36.942543.

3. E. G. Njoku, W. J. Wilson, S. H. Yueh, et al., "Observations of Soil Moisture Using A Passive and Active Low-Frequency Microwave Airborne Sensor During SGP99," *IEEE Transactions on Geoscience and Remote Sensing*, **40**, 12, December, 2002, pp. 2659–2673, doi: 10.1109/TGRS.2002.807008.

4. G. Macelloni, S. Paloscia, P. Pampaloni, et al. "The SIR-C/X-SAR Experiment on Montespertoli: Sensitivity to Hydrological Parameters," *International Journal of Remote Sensing*, **20**, 13, November, 2010, pp. 2597–2612, doi:10.1080/014311699211958.

5. F. Mattia, M. W. J. Davidson, T. Le Toan, et al. "A Comparison Between Soil Roughness Statistics Used in Surface Scattering Models Derived from Mechanical and Laser Profilers," *IEEE Transactions on Geoscience and Remote Sensing*, **41**, 7, August 2003, pp. 1659–1671, doi:10.1109/tgrs.2003.813359.

6. N. Baghdadi, M. Zribi, C. Loumagne, et al. "Analysis of Terrasar-X Data and Their Sensitivity to Soil Surface Parameters Over Bare Agricultural Fields," *Remote Sensing of Environment*, **112**, 12, June, 2008, pp. 4370–4379, doi:10.1016/j.rse.2008.08.004.

7. M. Brogioni, S. Pettinato, G. Macelloni, et al. "Sensitivity of Bistatic Scattering to Soil Moisture and Surface Roughness of Bare Soils," *International Journal of Remote Sensing*, **31**, 15, September, 2010, pp. 4227–4255, doi:10.1080/01431160903232808.

8. Kun-Shan Chen, *Radar Scattering and Imaging of Rough Surfaces: Modeling and Applications with* MATLAB@ , CRC Press, FL, USA, 2020.

9. H. Lievens, H. Vernieuwe, J. Álvarez-Mozos, et al. "Error in Radar-Derived Soil Moisture Due to Roughness Parameterization: An Analysis Based on Synthetically Surface Profiles," *Sensors*, **9**, 2, February, 2009, pp. 1067–1093, doi: 10.3390/s90201067.

10. W. Dierking, "Quantitative Roughness Characterization of Geological Surfaces and Implications for Radar Signature Analysis," *IEEE Transactions on Geoscience and Remote Sensing,* **37**, 5, September, 1999, pp. 2397–2412, doi: 10.1109/36.789638.

11. M. Zribi, V. Ciarletti, O. Taconet, et al. "Characterization of the Soil Structure and Microwave Backscattering Based on Numerical Three-Dimensional Surface Representation: Analysis with A Fractional Brownian Model," *Remote Sensing of Environment,* **72**, 2, May, 2000, pp. 159–169, doi: 10.1016/S0034-4257(99)00097-8.

12. Q. Li, J. C. Shi, K. S. Chen, "A Generalized Power Law Spectrum and Its Applications to the Backscattering of Soil Surfaces Based on the Integral Equation Model," *IEEE Transactions on Geoscience and Remote Sensing,* **40**, 2, February, 2002, pp. 271–280, doi:10.1109/36.992784.

13. M. M. Rahman, M. S. Moran, D. P. Thoma, "A Derivation of Roughness Correlation Length for Parameterizing Radar Backscatter Models," *International Journal of Remote Sensing,* **28**, 18, September, 2007, pp. 3995–4012, doi:10.1080/01431160601075533.

14. I. Champion, "Simple Modelling of Radar Backscattering Coefficient over A Bare Soil: Variation with Incidence Angle, Frequency and Polarization," *International Journal of Remote Sensing*, **17**, 4, April, 2007, pp: 783-800, March, 1996. doi: 10.1080/01431169608949045.

15. M. Zribi , O. Taconet , S. Le Hégarat-Mascle, et al. "Backscattering behavior and simulation comparison over bare soils using SIR-C/X-SAR and ERASME 1994 data over Orgeval," *Remote Sensing of Environment*, **59**, 2, June, 1997, pp. 256-266. doi : 10.1016/S0034-4257(96)00158-7.